

# Experimental Studies of Electron Affinity and Work Function from Aluminium on Oxidized Diamond (100) and (111) Surfaces

Michael C. James, Mattia Cattelan, Neil A. Fox, Rui F. Silva, Ricardo M. Silva, and Paul W. May\*

Three different procedures are used to deposit aluminium onto O-terminated (100) and (111) boron-doped diamond, with the aim of producing a thermally stable surface with low work function and negative electron affinity. The methods are 1) deposition of a  $> 20$  nm film of Al by high-vacuum evaporation followed by HCl acid wash to remove excess metallic Al, 2) deposition of  $< 3$  Å of Al by atomic layer deposition, and 3) thin-film deposition of Al by electron beam evaporation. The surface structure, work function, and electron affinity are investigated after annealing at temperatures of 300, 600, and 800 °C. Except for loss of excess O upon first heating, the Al + O surfaces remain stable up to 800 °C. The electron affinity values are generally between 0.0 and  $-1.0$  eV, and the work function is generally  $4.5 \pm 0.5$  eV, depending upon the deposition method, coverage, and annealing temperature. The values are in broad agreement with those predicted by computer simulations of Al + O (sub)monolayers on a diamond surface.

## 1. Introduction

The superlative properties of diamond, together with its ability to form a negative electron affinity (NEA) surface, are of interest for numerous electron-emission applications,<sup>[1]</sup> such as photodiodes,<sup>[2]</sup> electron sources,<sup>[3]</sup> secondary-electron-emission devices,<sup>[4]</sup> and thermionic energy conversion.<sup>[5]</sup> Similarly, low-work-function diamond devices have potential for applications such as photoelectrochemical CO<sub>2</sub> conversion.<sup>[6]</sup>

In order for an electron to be emitted from a metal surface, it must possess sufficient kinetic energy to overcome the potential barrier (or work function,  $\phi$ ), situated at the surface–vacuum interface. For semiconductors, the electrons reside in the valence band (VB) and so require additional energy (equivalent to that of the bandgap) to first excite them into the conduction band (CB) before they can be emitted. The work function is defined as the energy difference between the Fermi level (the electrochemical potential of electrons inside the material) and that of the vacuum level and is typically a few eV for most metals and semiconductors. Therefore, high-energy (e.g., UV) photons or temperatures  $> 1500$  K are usually required to provide sufficient energy for electron emission. For some semiconductors and insulators, however, the work function can be greatly reduced because in these materials, the conduction band minimum (CBM) is higher in energy than the vacuum level. This situation is known as NEA. Here, electrons located in the CB have no emission barrier to overcome to escape the surface. Bulk electrons residing in the VB, or in mid-bandgap states because of doping, only require enough energy (via photon absorption, thermalization, or electric fields) to excite them into the CB for emission to take place. Consequently, such NEA materials, which include diamond, cubic boron nitride,<sup>[7]</sup> AlN, and AlGaN,<sup>[8]</sup> are highly desirable for next-generation electron-emission applications. Because these are all wide-bandgap materials, the advantages of NEA might be outweighed by the high energies needed to excite electrons from the VB into the CB. However, this problem can be reduced if the NEA is sufficiently large and negative, i.e., has a value approaching that of the bandgap, and also by using suitable doping strategies, especially n-type, that raise the Fermi level and decrease the effective bandgap.<sup>[1]</sup>

Dr. M. C. James, Dr. M. Cattelan, Prof. N. A. Fox, Prof. P. W. May  
School of Chemistry  
University of Bristol  
Cantock's Close, Bristol BS8 1TS, UK  
E-mail: Paul.May@bristol.ac.uk

Dr. M. C. James  
Bristol Centre for Functional Nanomaterials  
H.H. Wills Physics Laboratory  
University of Bristol  
Tyndall Avenue, Bristol BS8 1TL, UK

Prof. N. A. Fox  
School of Physics  
H.H. Wills Physics Laboratory  
University of Bristol  
Tyndall Avenue, Bristol BS8 1TL, UK

Dr. R. F. Silva, Dr. R. M. Silva  
CICECO  
Department of Materials and Ceramic Engineering  
University of Aveiro  
3810-193 Aveiro, Portugal

 The ORCID identification number(s) for the author(s) of this article can be found under <https://doi.org/10.1002/pssb.202100027>.

© 2021 The Authors. Physica status solidi (b) basic solid state physics published by Wiley-VCH GmbH. This is an open access article under the terms of the Creative Commons Attribution License, which permits use, distribution and reproduction in any medium, provided the original work is properly cited.

DOI: 10.1002/pssb.202100027

In the case of diamond, to form an NEA surface it is necessary to terminate the diamond surface with atoms or groups of atoms that are electropositive relative to the bulk material, forming an electric dipole perpendicular to the surface, with positive charge outermost.<sup>[9]</sup> For diamond, H termination gives an NEA for each of the (100), (111), and (110) surfaces.<sup>[10–12]</sup> However, H-terminated diamond surfaces suffer from hydrogen desorption at elevated temperatures ( $\gtrsim 700$  °C).<sup>[13,14]</sup> This makes H-terminated diamond problematic for use in high-temperature applications, such as thermionic energy converters, and therefore there is an extensive ongoing search for alternative diamond-termination schemes that provide high NEA while remaining stable above 1000 K.<sup>[1]</sup>

The H-terminated diamond surface can be functionalized relatively easily by modifying the C–H bonds using a variety of standard wet chemistry and plasma techniques,<sup>[15]</sup> to produce new NEA surfaces with improved emission behavior and thermal stability. Previous experimental and computational studies of NEA surfaces on diamond include the use of Group I and II metals<sup>[16–19]</sup> and first-row transition metals (TMs)<sup>[20–24]</sup> as the electropositive species, with monolayer (ML) or sub-ML coverage on bare or oxidized diamond surfaces. Group I elements have long been known to exhibit NEA characteristics on diamond; however, larger adsorbed Group I elements have low thermal stability, which limits their usefulness at higher temperatures. For example, despite an extremely low work function of  $\approx 1.5$  eV, CsO-terminated diamond loses Cs through desorption above  $\approx 400$  °C; hence, the NEA is lost.<sup>[16]</sup> Recent computational and experimental work has focused upon elements that can provide a more robust surface in addition to NEA, especially smaller Group I and II metals, such as Li and Mg,<sup>[25–28]</sup> as well as various first-row TMs, including Cu, Ni, Ti, and Zn.<sup>[23,28]</sup> Results suggest that for metals deposited directly onto the diamond surface, carbide-forming TMs give a larger NEA. However, many elements do not readily form bonds with carbon, whereas others prefer bonding to oxygen and so the metal layer rapidly oxidizes on exposure to air. Some of these problems associated with the metal–diamond system can be overcome by depositing the metal onto an already oxidized diamond surface.<sup>[25]</sup> While it may appear counterintuitive to surface terminate with electronegative oxygen, provided a sufficiently electropositive metal is bonded on top of the oxygen layer, the overall combination can produce a net NEA. Other diamond terminations, such as Si, Ge, metal nitrides, amines, and OH groups, have also been studied, with varying degrees of success, all reviewed in the study by James et al.<sup>[1]</sup>

To date, aluminium on the diamond surface has been rarely studied for its NEA properties, even though Al forms a carbide and bonds sufficiently well to a diamond surface to act as either Schottky or ohmic contacts for diamond-based devices.<sup>[29]</sup> Al<sub>2</sub>O<sub>3</sub> layers on diamond are candidates for device interfaces in metal–oxide–semiconductor field-effect transistors (MOSFETs)<sup>[30]</sup> and capacitors (MOSCAPs)<sup>[31]</sup> and additionally for passivation of the p-type conductive surface on H-terminated diamond resulting from surface transfer doping.<sup>[32]</sup> However, these layers are typically much thicker than the sub- or few MLs required to give NEA.

The Al–O–diamond system has recently been studied computationally on both the (100) and (111) diamond surfaces.<sup>[33–35]</sup>

Al adsorption onto O-terminated diamond was predicted to give large adsorption energies (from  $-6.0$  to  $-7.3$  eV) on both (100) and (111) diamond at 0.25 ML Al coverage due to the strong ionic bond between Al and O, as well as NEA values as large as  $\approx -2.2$  eV. However, at higher coverages, some Al–Al metallic bonding occurs, making Al less ionic and the surfaces mostly of positive electron affinity (PEA). Adsorption energies decreased with increasing Al coverage, which help avoid island formation of the metal on the surface. Another study of different Al:O ratios on diamond also calculated some of them to exhibit NEA but with similar adsorption energy with respect to bulk Al<sub>2</sub>O<sub>3</sub>.<sup>[36]</sup>

In this article, we report experimental results from the Al–O–diamond system, including measurements of work function and EA from different diamond surfaces, coverages, and preparation procedures.

## 2. Experimental Section

Polycrystalline boron-doped diamond (BDD) samples of  $10 \times 10$  mm<sup>2</sup> were used in preliminary experiments to explore the effectiveness of the thick-film Al deposition process (see Section 2.3). BDD is required to make the surface conductive and prevent surface-charging effects during characterization procedures that rely on electron emission from the sample, such as X-ray photoemission spectroscopy (XPS). Conducting n-type silicon (100) substrates (Si-Mat, e.K.) were seeded with 1–5 nm nanodiamond using an electro-spray procedure, as detailed in the study by Fox et al.<sup>[37]</sup> A BDD layer was then grown on this to a thickness of  $\approx 1$   $\mu$ m using a standard hot-filament chemical vapor deposition (CVD) system. 1% CH<sub>4</sub>/H<sub>2</sub> plus 40 ppm of B<sub>2</sub>H<sub>6</sub> (relative to H<sub>2</sub>) was used as the process gas mixture at a total gas flow of 200 sccm and a process pressure of 20 torr. The substrates were placed on a heated substrate holder of  $\approx 4$  mm beneath three tantalum filaments inside a vacuum chamber. Typically, 25 A was passed through the filaments to bring them to a temperature of  $\approx 2100$  K (measured by a two-color optical pyrometer). Radiative heat from these filaments, plus additional heating from the substrate heater, maintained the substrate at a temperature of  $\approx 850$  °C for the duration of deposition (typically 1–3 h). BDD overlayers grown in the same reactor under the same conditions has previously been shown<sup>[38]</sup> to contain a boron concentration of up to  $\approx 10^{20}$  cm<sup>-3</sup>, measured from a depth profile using secondary-ion mass spectroscopy, making them of near-metallic conductivity.

For more detailed experiments, single-crystal diamond substrates were purchased from Element Six, Ltd (Ascot, UK). These included square, CVD-grown, undoped (100) substrates (product code: 145-500-0248) with a surface polished to an average roughness of  $\approx 3.9$  nm (as measured by atomic force microscopy), and a side-length of 3 mm, and undoped triangular (111) substrates (product code: MM 111/4010) grown by the high-pressure high-temperature (HPHT) method with a surface polished to 20.1 nm roughness and a side length of 4 mm. A conducting BDD overlayer ( $\approx 1$   $\mu$ m) was grown homoepitaxially on these crystals using hot-filament CVD to make the surface conductive, as described earlier.

## 2.1. Cleaning and Hydrogen Termination

Diamond surfaces were cleaned by refluxing in an acid solution (6.5 g  $\text{KNO}_3$  in 100 ml of 95%  $\text{H}_2\text{SO}_4$ ) for 6 h to remove particulate residues that were left over from the polishing process. The diamond samples were then rinsed thoroughly with deionized water. To ensure all samples started out with identical fully hydrogenated surfaces, the cleaned diamond substrates were placed into a microwave CVD reactor and a hydrogen plasma was used to rehydrogenate the surface in a multistep process, as described in the study by Wan et al.<sup>[39]</sup>

## 2.2. Oxygen Termination

Two different methods were used to convert the H-terminated diamond into oxygen termination: UV/ozone treatment or oxidation using an atomic layer deposition (ALD) system. In each case, the oxidation times and process conditions were chosen to maximize oxygen coverage on the surface. For UV/ozone treatment, diamond samples were positioned  $\approx 4$  cm below a mercury lamp in a Jelight UVO cleaner. Air was passed over the samples, which were illuminated with 256 nm UV light at room temperature and pressure for 30 min.

The ALD oxidation procedure was conducted at the University of Aveiro in Portugal using  $\text{H}_2\text{O}$  (Milli-Q ultrapure water) as an oxidizing species. Details of the ALD chamber have been published previously.<sup>[40]</sup> For the oxidation procedure, samples were first heated to 200 °C at 400 mtorr for 20 min in flowing dry  $\text{N}_2$  gas (20 sccm) to desorb any unwanted adsorbates. Oxidation was conducted by introducing into the chamber a set number of pulses of  $\text{H}_2\text{O}$  (pulse time length of 2 s) and pumping this out after a fixed time. Two oxidation recipes were tested, a short one (one pulse of  $\text{H}_2\text{O}$  for 1 min) and a long one (two pulses for 5 min). Subsequently, the temperature of the ALD chamber was increased to 300 °C for the heat treatment of the samples for a period of 1 h under vacuum. The samples were then cooled down to room temperature in  $\text{N}_2$  atmosphere.

## 2.3. Aluminium Deposition

Three methods were used to deposit aluminium onto the oxidized diamond samples: high-vacuum thermal evaporation, ultrahigh vacuum (UHV) electron beam evaporation, and ALD. **Figure 1a** shows the so-called thick-film process, which involves the thermal evaporation of Al in a high-vacuum chamber for a fixed time, resulting in deposition of over 20 nm of Al. Samples were then thermally annealed at 300 °C for 1 h at a pressure of  $10^{-8}$  mbar to encourage covalent bonding between Al and the oxidized diamond surface. The sample was then washed in 0.1 M  $\text{HCl(aq.)}$  for 20 h to remove any excess Al that had not chemically bonded to the surface O layer. This process is similar to the one reported by O'Donnell et al.<sup>[27]</sup> to produce LiO-terminated diamond samples and in a preliminary study investigating NEA from Ti, Cr, and Al layers on oxidized polycrystalline diamond.<sup>[41]</sup> A drawback to this method is that the sample must be transferred from the evaporation system to the UHV analysis chamber, with the possibility of contamination or modification of the surface by exposure to ambient air.

The thin-film method (Figure 1b) has been used previously to prepare LiO-,<sup>[27]</sup> MgO-,<sup>[28]</sup> VO-,<sup>[42]</sup> and Si- and Ge-terminated diamond.<sup>[43,44]</sup> It involves the electron beam deposition of a thin (ML or sub-ML) metal layer under UHV followed by an in situ anneal at a temperature of at least 600 °C. The anneal creates a strong covalent bond between the oxygen or carbon surface atoms and any adjacent overlying metal atoms, while any excess, unbonded metal thermally desorbs and is pumped away. An advantage of this method is that the metal layer can be deposited in the same vacuum system as the analysis. This makes sequential deposition, annealing and analysis steps possible without breaking vacuum.

To calibrate one ML of Al deposition onto diamond, it was calculated that the deposition of 2.34 Å of Al is equal to one ML as this is the separation between the (111) planes in bulk Al. This was checked against the Al atomic percentage measured using XPS using Al-terminated (100) and (111) single-crystal diamond samples. These samples were first heated to 950 °C for 10 min in UHV, and XPS confirmed that after this procedure, no signal

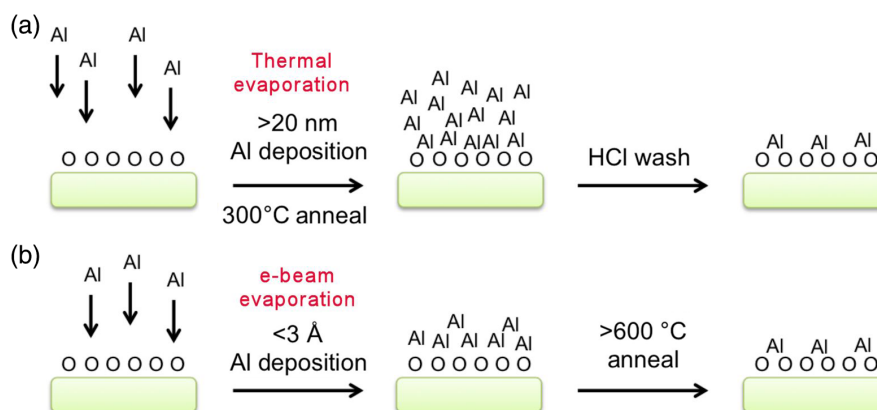


**Figure 1.** a) The thick-film method deposits a thick metal layer onto O-terminated diamond, and excess metal is washed off, leaving a (sub)monolayer of metal chemically attached to the surface. b) The thin-film method deposits a (sub)monolayer of metal that is “activated” by thermal annealing.

from elements other than carbon was obtained from the surface, within the detection limit for the XPS system ( $\approx 1\%$ ). Al was then e-beam deposited onto these samples, without breaking vacuum. After deposition of one ML of Al, the relative atomic percentages of Al were measured by XPS to be 6.3% and 6.5% for the (100) and (111) surfaces, respectively. This was in excellent agreement with our previously calculated value for one ML of Al on a  $(1 \times 1)$  oxygen surface reconstruction on diamond.

The final technique to deposit thin layers of Al onto O-terminated diamond was ALD, again conducted at the University of Aveiro in Portugal. Samples of oxygen-terminated diamond were prepared in one of the two ways mentioned in Section 2.2 and were placed into the ALD chamber, which was pumped out, and the sample surface was heated to 200 °C and outgassed as before in dry  $N_2$ . With the samples remaining at 200 °C, one pulse of gaseous trimethylaluminum ( $Al(CH_3)_3$ , 97% from Sigma Aldrich) was introduced (pulse time length of 2 s) and pumped away after 1 min. After deposition, the samples were annealed at 300 °C under vacuum for 1 h to react Al with the O-terminated diamond and then cooled down to room temperature in  $N_2$  atmosphere following the same approach as the ALD oxidation procedure. This annealing process was conducted to reduce the surface reactivity with ambient air, thereby allowing the samples to be sent to the UK (a period of  $\approx 1$  week).

## 2.4. Film Analysis

Scanning electron microscopy (SEM) images were obtained using a JEOL JSM IT-300 microscope. The BDD layer deposited on the surface of the diamond made them sufficiently conductive to prevent charging effects under the electron beam.

Photoemission spectroscopy and surface diffraction film characterization were conducted at the Bristol University NanoESCA II Facility. XPS was used to obtain the elemental composition of the first few atomic layers of the samples. The relative amounts of each element, and their atomic percentage coverage, were determined via calibration using the peak area for each element and its sensitivity factor (available from XPS literature<sup>[45]</sup>). A monochromatic Al  $K\alpha$  X-ray source (1486.7 eV) was used, with an overall energy resolution of 600 meV at a pass energy of 20 eV. The XPS binding energy scale was calibrated by aligning the Au  $4f_{7/2}$  peak to 84.0 eV using a polycrystalline gold film.

Ultraviolet photoelectron spectroscopy (UPS) was used to study the valence band electrons. A UPS spectrum typically shows a large peak at high binding energy from secondary-electron emission. Other peaks give information on the electron density of states. NEA can be observed by the presence of an additional secondary-electron emission peak component at a higher binding energy, arising from the additional secondary-electron population exceeding the vacuum energy.<sup>[39]</sup> This is possible as real surfaces contain some mid-bandgap states just below the CB for the electrons to occupy. The work function,  $\phi$ , was calculated from the difference between the photon energy and the emission onset for PEA surfaces. UPS was also used to determine the difference between  $E_F$  and the energy of the valence band maximum,  $E_{VBM}$ . This allows the EA,  $\chi$ , to be approximated from

$$\chi = \phi + (E_F - E_{VBM}) - E_g \quad (1)$$

where  $E_g$  is the bandgap of the material.

Region-selected UPS was conducted using energy-filtered photoemission electron microscopy (EF-PEEM) with a monochromatized He-I light source (21.2 eV) in the NanoESCA II system. Photoemitted electrons were filtered by kinetic energy in the first hemisphere of an imaging double-hemisphere energy analyzer, and the signal was amplified using a Channeltron. The energy resolution of this technique was 0.14 eV. An iris allowed UPS to be conducted on a region of interest of area  $\approx 200 \mu m^2$ .

EF-PEEM was also used to extract a map of the work function across a sample surface. As in UPS, photon excitation emits electrons from the substrate under UHV, and the emitted electrons are energy filtered using an imaging double-hemisphere energy analyzer. For EF-PEEM, images were obtained for successive energies, allowing the work function at different locations to be visualized as a color-coded map, with an energy resolution of 0.14 eV and a spatial resolution of  $\approx 150$  nm. The UV light source was the same monochromatic He-I lamp used for UPS. Photoelectrons were extracted from the sample by applying a bias of 7–12 kV across the sample-to-extractor electrode distance of  $\approx 1.8$  mm. Lower extraction voltages were sometimes required to prevent sudden field-induced electron discharge from the sample due to localized surface-charging effects. The work function values were then corrected for the Schottky effect of 98 meV, resulting from the high PEEM extractor field.<sup>[46]</sup>

Spot profile analysis low-energy electron diffraction (SPA-LEED) was also used to study the surface structure and crystallinity of the diamond samples. The SPA-LEED system used 170 eV electrons and a Channeltron detector.

To ensure that the measurements in this work originated from AlO-terminated diamond and not from the Al layers, the same experimental procedures were previously used to study bare, H-terminated, and O-terminated diamond as reference or control samples. These results can be found in the study by James.<sup>[33]</sup>

## 3. Results

### 3.1. Thick-Film Al + O Diamond Preparation

Preliminary experiments to confirm the efficacy of the thick-film process (Section 2.3) were conducted using two polycrystalline BDD samples that were previously surface oxidized using the UV/ozone method (Section 2.2). Al was deposited on these, and one sample was annealed in high vacuum at 300 °C for 1 h after Al deposition, whereas the other sample was not annealed. Post-deposition, the presence of Al was clearly visible as a shiny metallic coating on the surface of both samples. After 1 h of acid etching, the metallic surface looked less uniform, and after 20 h, no trace of the metallic surface remained visible to the naked eye on either sample. SEM analysis (see Figure S1, Supporting Information) showed that the surface appearance after acid treatment was indistinguishable from that of the as-grown oxidized sample, suggesting that excess Al was cleaned from the surface.

The presence of an Al peak in XPS confirmed that some Al remained on the surface after acid cleaning, although the thickness of the Al layer was unknown. We can estimate, however,

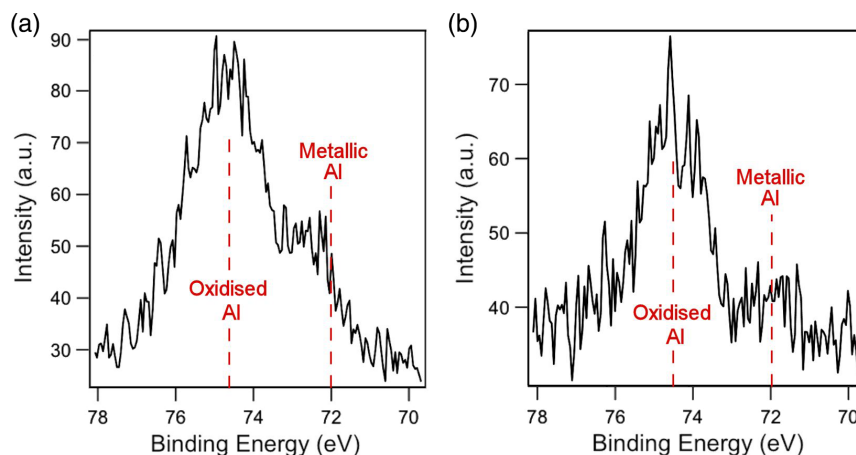


**Figure 2.** XPS spectra of the Al 2*p* peak for the two polycrystalline Al + O-terminated BDD samples. a) Unannealed sample and b) annealed sample, both prepared by the thick-film process.

that the Al thickness must be between a ML and  $\approx 10$  nm, which is the resolution of the SEM used to image the facets in Figure S1 (Supporting Information). **Figure 2** shows the XPS analysis of the Al 2*p* peak for the annealed and unannealed Al + O-terminated diamond samples. The Al 2*p* peak has a small spin-orbit splitting ( $<0.5$  eV) and so appears as a single peak within the resolution of the XPS instrument. The presence of the Al 2*p* peak in both instances indicates that some Al remains on the surface after the cleaning procedure and that the Al + O termination is both air and water stable, even with no annealing. For both spectra there are two Al 2*p* environments; the lower binding-energy peak at 72.0 eV is attributed to metallic Al and the higher binding-energy peak at 74.5 eV to oxidized Al.<sup>[47]</sup> There is a significant decrease of the metallic component with annealing, suggesting that annealing increased the aluminium-oxygen bonding and/or removed some more unbonded excess Al. A further sample was prepared using the same thick-film procedure, except that half of the sample was masked such that Al was deposited only on the exposed half. XPS spectra of the two sides of the surface showed that Al was only present on the side where deposition had occurred. This indicated that Al did not migrate during the acid-washing step.

Following the successful creation of an Al + O termination by the thick-film process on polycrystalline diamond, next, the properties of Al + O termination on single-crystal diamond (100) and (111) surfaces were studied in more detail. The Al + O terminations were prepared in the same manner as described earlier, and both samples were fully characterized after annealing for 10 min under UHV conditions at three different temperatures. The lowest temperature, 300 °C, was the temperature used for sample degassing upon introduction to the UHV system. Higher annealing temperatures of 600 °C and 800 °C were selected as they can give an indication of the change in surface characteristics within the expected temperature range for thermionic emission.

**Figure 3** shows normalized XPS spectra of the C 1*s*, O 1*s*, and Al 2*p* peaks for (100) and (111) single-crystal diamond surfaces at each annealing temperature. The oxidized C 1*s* peak comprises bulk and surface C-C bonding component peaks, plus C-O and C=O component peaks at higher binding energies.<sup>[31,48,49]</sup> The O

1*s* peak is expected to be a complex combination of the ether, ketone, and hydroxyl peaks<sup>[50]</sup> in addition to an Al-O peak. An Al-O component peak would be expected at a similar binding energy to the hydroxyl peak ( $\approx 531.0$  eV).<sup>[47]</sup>

The C 1*s* peak did not notably change in shape for the (100) sample, but there was a decrease in the C-O and C=O components of the C 1*s* peak between the 300 and 600 °C annealing for the (111) sample (Figure 3b). None of the C 1*s* peaks here or later contained a carbide component, which would have been observed at a binding energy of  $\approx 282$  eV.<sup>[47]</sup> The O 1*s* peak for the (100) sample showed a relatively large increase in a low binding-energy component with temperature (Figure 3c); this is attributed to an increase in the Al-O component peak.

For both the (100) and (111) samples, the Al 2*p* peak was centered at  $\approx 74.5$  eV, indicating that Al was coordinated with bonded oxygen (Figure 3e-f). There was a slight metallic Al component at a lower binding energy for the (100) sample,  $\approx 20\%$  of the total peak area at each temperature, like that seen in the polycrystalline samples. No metallic Al peak was observed for the (111) sample.

With increasing annealing temperature, both samples showed a slight shift of all three peaks to higher binding energies. This could be due to increasing downward band bending at the surface, caused by a change in surface states.<sup>[51]</sup>

Quantitative surface composition was determined using prior calibration of the XPS sensitivity for the elements concerned (see Section 2.4). The total amount of Al was similar between the two samples, just over 1%, and this value remained constant at all annealing temperatures, suggesting that Al was strongly bonded to the surface. The O atomic percentage was 6–7% for the (100) surface, which is equivalent to 1 ML coverage for O-terminated diamond, suggesting that Al is present at sub-ML coverage here. For the (111) surface, the O percentage was 14–16%, larger than expected, and this was attributed to additional O bonded to Al, possibly from air or water exposure. This C-O-Al-O bonding arrangement would be expected to have a detrimental effect by increasing the work function and EA as it would form an additional dipole with negative charge outermost from the surface. The atomic percentage of O on both surfaces did not show

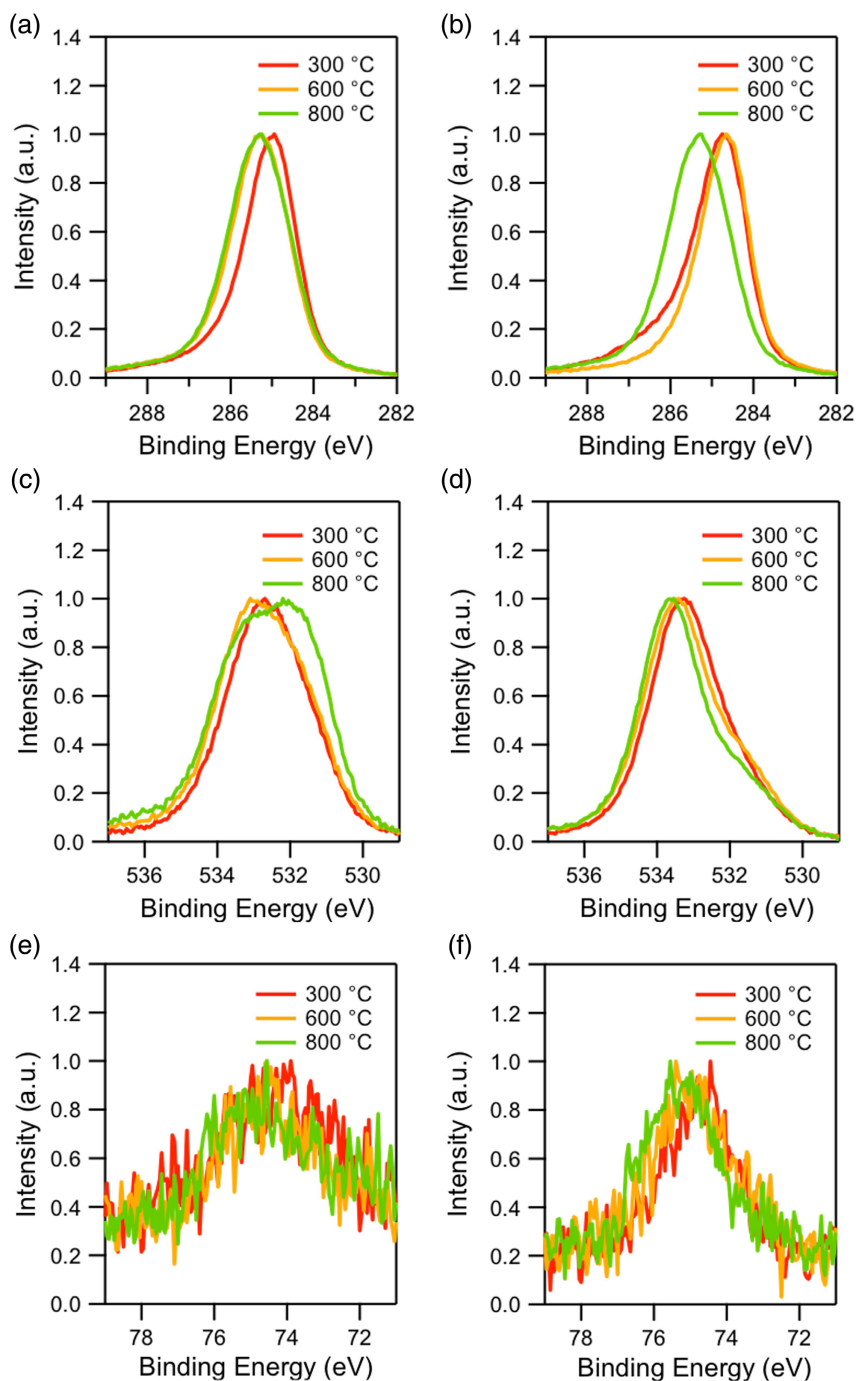


**Figure 3.** XPS spectra of a,b) C 1s, c,d) O 1s, and e,f) Al 2p peaks at different annealing temperatures for thick-film-prepared Al + O-terminated diamond. (a), (c), (e) are from the (100) surface, and (b), (d), (f) are from the (111) surface. The peak heights have all been normalized to the same maximum intensity.

any obvious trend with temperature, meaning that O was also strongly bonded to the surface.

The work function across the surface was measured after each of the annealing steps. Shown in **Figure 4** are work function maps for both the (100) and (111) surfaces, and the values are shown in **Table 1**. Starting with the (100) surface, after the 300 °C anneal, the work function was just under 4.7 eV and

was relatively uniform across the surface, except for a few regions where it was just below 4.0 eV. After the 600 °C anneal, the work function decreased between 3.7 and 4.3 eV. After the 800 °C anneal, there was a relatively constant work function between 4.0 and 4.2 eV across the surface. The (111) surface, meanwhile, exhibited the lowest work function after the 300 °C anneal, with a relatively uniform value of  $\approx 4.1$  eV. This increased to between

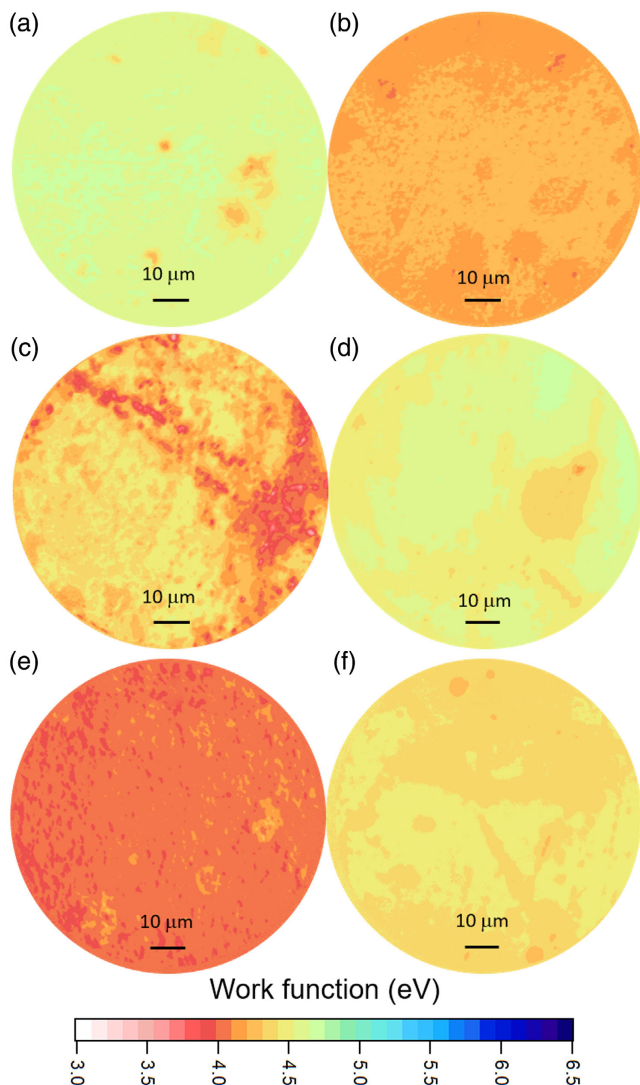


**Figure 4.** Color-coded work-function maps of Al + O-terminated diamond prepared by the thick-film procedure, after annealing at a,b) 300 °C, c,d) 600 °C, and e,f) 800 °C. (a), (c), and (e) show the (100) surface, whereas (b), (d), and (f) show the (111) surface.

**Table 1.** Work-function values and electron affinities measured for the (100) and (111) diamond surfaces prepared using the three different methods: the thick-film method, thin-film electron beam evaporation, and ALD. The range of values given in each case gives an indication of the uniformity across the sample. No measurements were made for the ALD-prepared (100) samples annealed at 600 and 800 °C due to excessive charging in the XPS, the reason for which is unknown.

Preparation	Surface	Work function [eV]			Electron affinity [eV]		
		Annealing temperature [°C]			Annealing temperature [°C]		
		300	600	800	300	600	800
Thick film	(100)	4.0–4.7	3.7–4.3	4.0–4.2	From –0.5 to +0.3	From –0.4 to +0.2	From –0.1 to +0.1
Thick film	(111)	4.1	4.2–4.6	4.2–4.5	From –0.4 to 0.0	From –0.4 to 0.0	From –0.3 to 0.0
ALD	(100)	3.9–4.0	–	–	–0.9	–	–
ALD	(111)	3.8	4.1	4.0–4.6	–0.8	–0.7	From –0.5 to –0.1
e-beam	(100)	4.0–4.8	3.5–4.1	4.3–5.0	From –0.1 to +0.7	From –1.8 to –1.3	From –0.3 to +0.4
e-beam	(111)	4.1–5.2	4.1–4.7	4.1–5.0	From –0.4 to +0.7	From –0.7 to –0.1	From –0.8 to +0.1

4.2 and 4.6 eV after the 600 °C anneal, with a similar range of 4.2–4.5 eV observed after the 800 °C anneal.

Shown in **Figure 5** are UPS spectra obtained after the 300 °C high-vacuum anneal. Here and later, the spectra were acquired from the lowest-work-function regions and were normalized by intensity of the valence band structure. Inset in the figure shows a magnified plot showing the fitting used to determine the energy of the valence band maximum,  $E_{VBM}$ , relative to the Fermi energy,  $E_F$ . The work function is determined by the difference between the UV photon energy and the onset of emission.

The secondary emission peak for the (100) sample was four times the height of that of the (111) sample. The (100) sample had a slightly more negative EA, calculated, using Equation (1), to be –0.5 eV compared with –0.4 eV for the (111) sample. Acquiring UPS spectra in different regions of the surface showed that  $E_F - E_{VBM}$  remained relatively constant. As such, most of the (100) surface (which showed a larger work function) exhibited a PEA of 0.3 eV.

UPS spectra were not obtained after higher-temperature anneals, but the EA values were still calculated from the work function maps by using the change in C 1s peak position from XPS to determine  $E_F - E_{VBM}$ ,<sup>[52]</sup> and are shown in Table 1.

### 3.2. Thin-Film Al + O Termination by ALD

Two BDD films were oxidized by the ALD technique (see Section 2.2) by introducing either one or two pulses of H<sub>2</sub>O for 1 min. Al was deposited on these samples by ALD (Section 2.3); then, the samples were annealed for 1 h at 300, 600, and 800 °C, as earlier. The first sample was (100) diamond, and XPS analysis showed that the Al and O coverages were 0.6–1.0% and 1.6–2.0%, respectively, both of which remained roughly constant with temperature. Because this O coverage was lower than optimal (1 ML), the second sample, now of (111) diamond, had two pulses of H<sub>2</sub>O compared with one for the previous (100) sample. XPS of this (111) film showed that the O coverage now increased to a relatively high value of 15.0% at 300 °C, which decreased to ≈8.0% by 600 °C, probably due to desorption of some excess oxygen. The corresponding Al coverage remained constant across the temperature range at ≈4%. Analysis of the XPS C 1s, O 1s, and

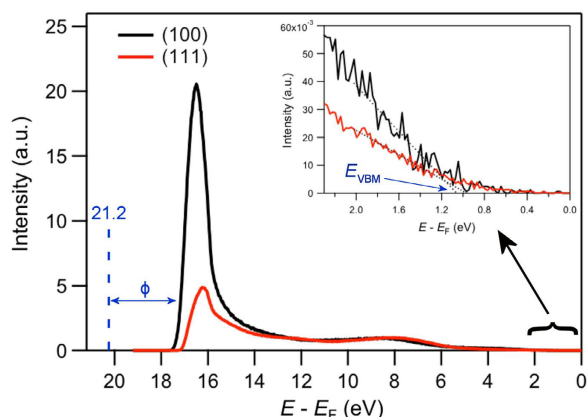


**Figure 5.** UPS spectra (He I excitation at 21.2 eV photon energy) acquired after a 300 °C anneal for Al + O-terminated (100) and (111) single-crystal diamond prepared by the thick-film procedure. The analyzed region is  $\approx 200 \mu\text{m}^2$ . Inset shows a magnified view of the fitting used to determine the VBM energy relative to the Fermi energy.

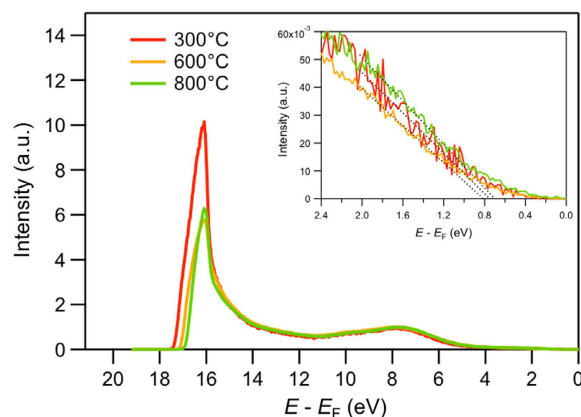


**Figure 7.** UPS spectra (He I, 21.1 eV photon energy) of Al + O-terminated (111) diamond prepared with the ALD procedure after annealing at the three temperatures.

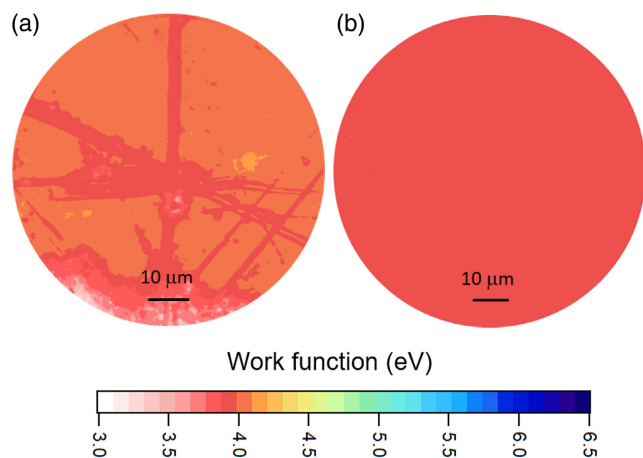


**Figure 6.** Color-coded work-function maps of Al + O-terminated diamond prepared by the ALD procedure after annealing at 300 °C for a) the (100) surface and b) the (111) surface.

Al  $2p$  peak shapes after annealing at the three temperatures showed that the peaks followed similar behavior to those for the thick film samples, as shown previously in Figure 3.

The work function after the three annealing temperatures was measured for both samples, see Table 1, with the lowest values being for the 300 °C anneal in both cases, as shown in Figure 6 (and also in Figure S2, Supporting Information).

Figure 7 shows UPS spectra for the (111) sample at each annealing temperature. The highest secondary-electron emission peak was observed after the 300 °C anneal. The calculated EA values are shown in Table 1.

### 3.3. Thin-Film Deposition by Electron Beam Evaporation

While using ALD for the deposition of Al and O gave some promising results, there was little controllability or consistency in the

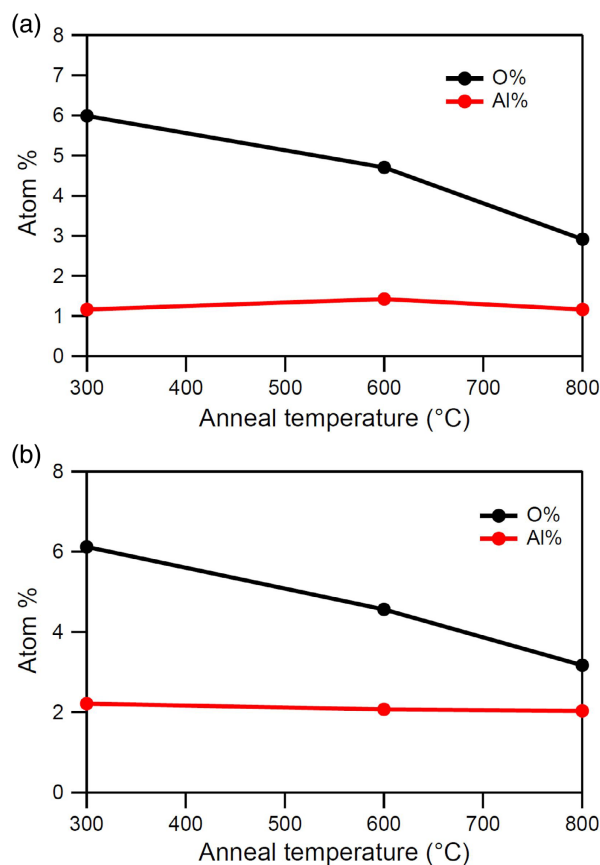


**Figure 8.** Atomic percentages of surface O and Al for Al + O-terminated a) (100) and b) (111) diamond prepared by electron beam evaporation. For both O and Al, a surface coverage of  $\approx 6\%$  corresponds to one ML.

amount of O or Al on the surface. Thus, the UHV electron beam evaporation technique (Section 2.3) was used to see if it would make a more reliable alternative. Al + O terminations were prepared by deposition of 0.25 ML Al (0.59 Å) onto (100) and (111) single-crystal diamond samples that were previously

O-terminated using the UV/ozone method (Section 2.2). This was followed by annealing at 300, 600, or 800 °C for 1 h.

**Figure 8** shows the relative atomic percentages of O and Al immediately after Al deposition and annealing at successive temperatures. There is a notable decrease in O atomic percentage for both (100) and (111) surfaces after each annealing step. It is unclear as to why the O desorbed so readily for these samples

but did not do so for the previous Al + O deposition methods. The Al atomic percentage, meanwhile, remained relatively constant in both cases,  $\approx 1.0$ – $1.4\%$  ( $\approx 0.17$  ML) for the (100) surfaces and  $\approx 2.0$ – $2.2\%$  ( $\approx 0.33$  ML) for the (111) surface.

Normalized XPS spectra for the C 1s, O 1s, and Al 2p peaks are shown in **Figure 9**. In both cases the Al 2p peak was centered at  $\approx 74.5$  eV, indicating that Al was oxidized. For the (100) sample,

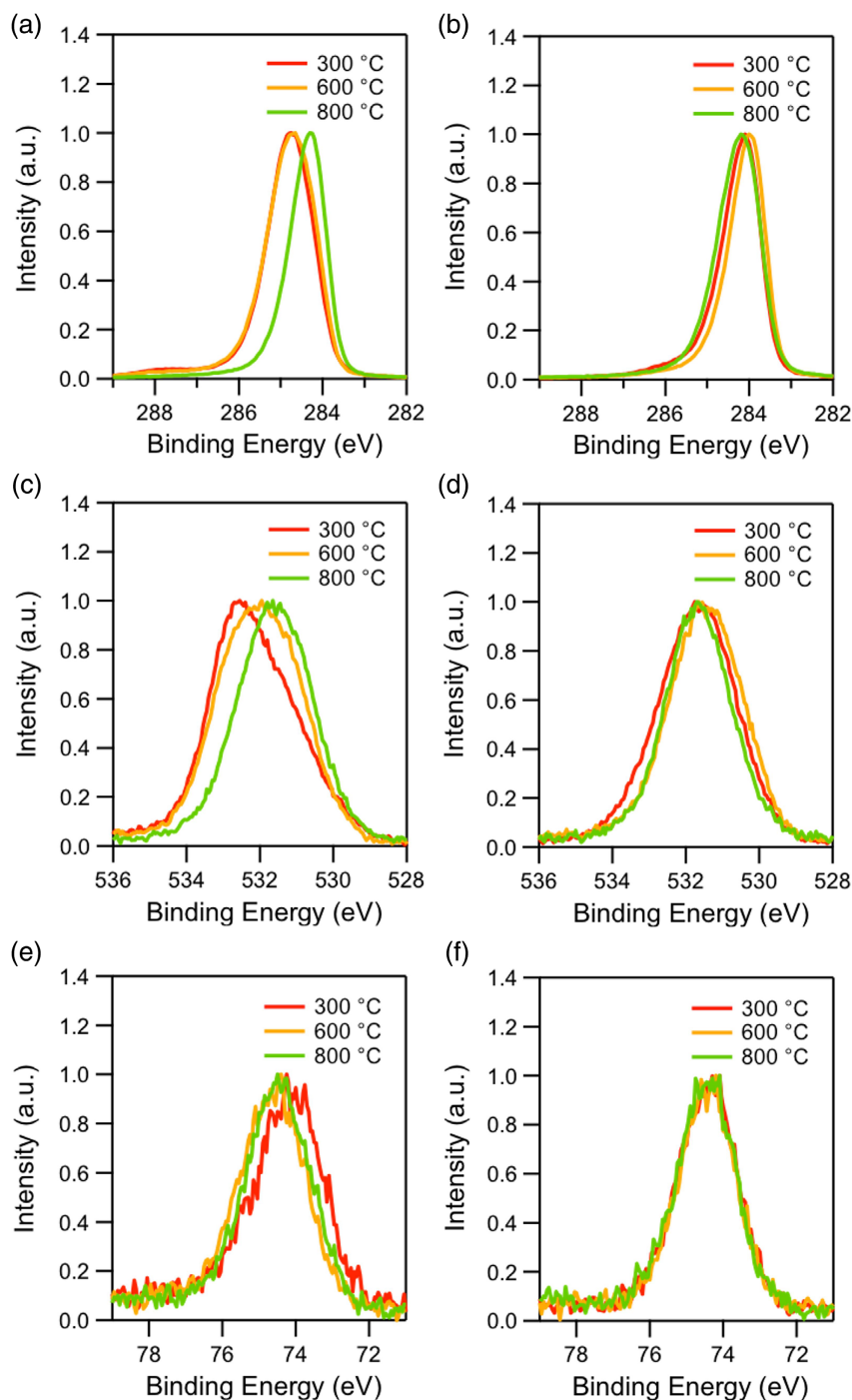


**Figure 9.** XPS spectra of a,b) C 1s, c,d) O 1s, and e,f) Al 2p peaks at different annealing temperatures for Al + O-terminated diamond prepared by electron beam evaporation. (a), (c), and (e) are from the (100) surface, whereas (b), (d), and (f) are from the (111) surface.

as previously observed, there was a large increase in the low-binding-energy component peak in the O 1s spectrum (Figure 9c), attributed to Al–O bonding. In this case, there was not an associated decrease in the C–O and C=O components of the C 1s peak. There was, however, a shift of the Al 2p peak to slightly higher binding energy after the 600 °C anneal, suggesting that here, oxygen remained bonded to carbon and bonded more strongly with Al. Each peak for the (111) sample, meanwhile, showed little change with successive annealing steps.

Work-function maps of these surfaces at different annealing temperatures are shown in Figure 10, and the values are shown in Table 1. The maps show that the work-function values are uniform over most of the analyzed area, except for a few roughly circular localized regions, where the work function is markedly different. These regions are artifacts that arise from macro-3D defects on the sample surface, such as scratches or hillocks. EF-PEEM is very sensitive to 3D structures; “hills” and “valleys”

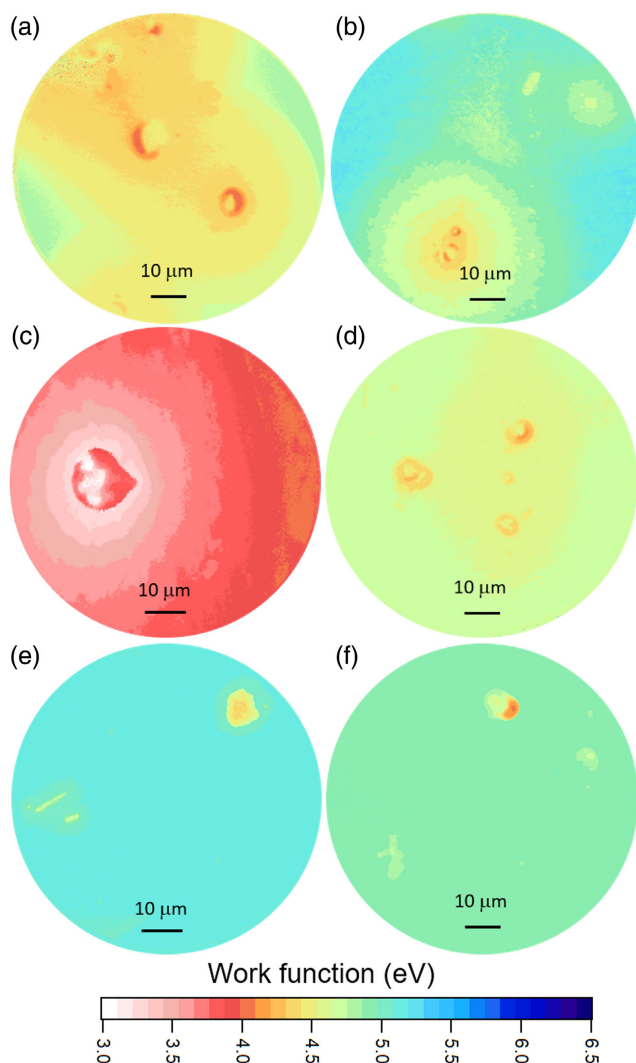


**Figure 10.** Color-coded work function maps of Al + O-terminated diamond prepared by electron beam evaporation, at annealing temperatures of a,b) 300 °C, c,d) 600 °C, and e,f) 800 °C. (a), (c), and (e) are for the (100) surface and (b), (d), and (f) are for the (111) surface.

have very different emission probabilities due to the variation in extraction field with distance, which appear on the work-function maps as regions of apparently higher or lower work function.

Figure 11 shows UPS spectra for the two surfaces at the different annealing temperatures. The (100) surface showed a relatively small secondary-electron emission peak after the 300 °C anneal, increasing in height with successive annealing steps. After the 600 °C annealing, the spectrum showed a broad multicomponent secondary-emission peak, and the Fermi level was close to the VBM position. In contrast, the (111) surface showed no variation of secondary-electron emission peak height. EA values for the two surfaces were determined from these spectra and are shown in Table 1.

SPA-LEED was also conducted on selected samples to determine whether any surface ordering had occurred (see Figure S3, Supporting Information). The quality of the electron beam deposition was also proven by the appearance, after the 800 °C anneal, of a faint (2 × 1) LEED pattern on the (100) surface, as predicted by computational experiments.<sup>[35]</sup> The (111) surface showed a (1 × 1) LEED pattern, consistent with computational calculations that predicted this to be the most stable structure.<sup>[35]</sup>

#### 4. Conclusion

Three different methods were used to deposit Al onto O-terminated diamond, with the intention of producing a thermally stable surface with low work function and NEA, with measured values shown in Table 1. Work-function maps indicated that the thick-film method gave a relatively uniform work function across the surface. This has previously been a problem reported for other metal–oxygen terminations prepared by this method<sup>[26]</sup> and so the better-than-expected uniformity here is attributed to the mild conditions and long reaction time used during the acid-wash step. NEAs were observed up to 800 °C, and there was little change in the O and Al amounts and peak shapes in XPS with increasing annealing temperatures.

The ALD-prepared samples showed particularly low work-function values after the 300 °C anneal, and work-function maps from this procedure exhibited the highest degree of uniformity. However, for the (100) surface, the low work function was not reproducible, and for the (111) surface, the work function increased significantly with temperature. In some cases, there was significant O and Al coverage on the surface, suspected to be from aluminium oxide deposition onto the surface rather than termination of the surface. Nevertheless, in some of these samples, the work function and EA were even lower than that observed for H-terminated diamond.

The electron beam evaporation method showed a much larger spatial variance of work function compared with the other two methods, suggesting that deposition was not uniform or there was agglomeration of Al upon annealing. Annealing resulted in a loss of oxygen from the surface and a significant change in work function. Nevertheless, low work functions and NEA were still observed, including after high-temperature annealing.

For each deposition procedure, the main issue with Al + O termination was determined to be the change in oxygen behavior rather than desorption of Al. For the thin-film-prepared samples, at higher temperatures, as much as 50% of the O coverage was

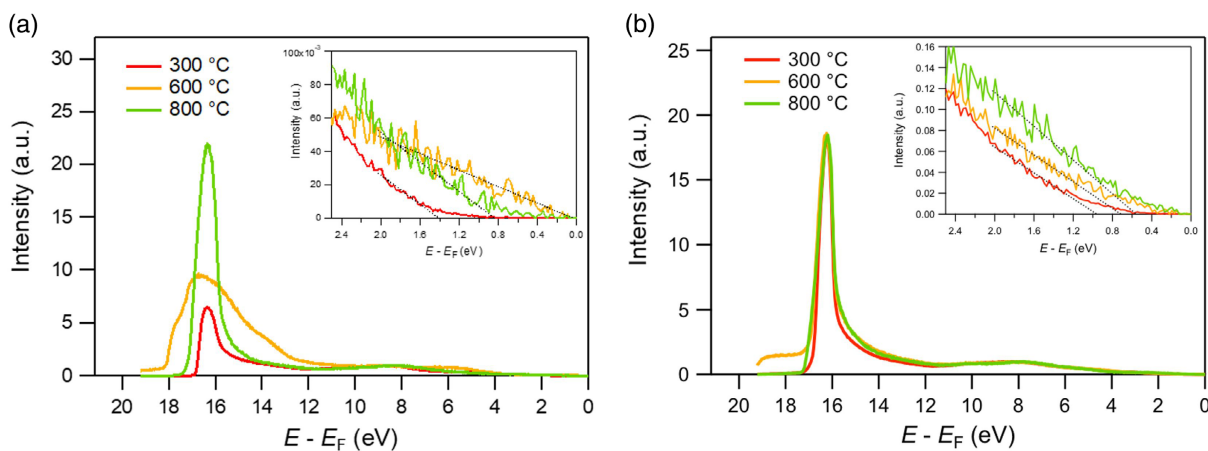


**Figure 11.** UPS spectra (He I, 21.1 eV photon energy) of Al + O-terminated a) (100) and b) (111) diamond prepared by electron beam evaporation. Inset shows a magnified view of the VBM energy relative to the Fermi energy.

lost. This was unexpected, both because O-terminated diamond is usually stable at  $\approx 900^\circ\text{C}$ <sup>[12,53]</sup> and because the thick-film-prepared samples did not suffer this issue. In addition, in many cases, the C–O and C=O component peaks of the C 1s spectra in XPS were observed to decrease slightly relative to that from the bulk  $sp^3$  carbon peak, and this was accompanied by an increase of a low-binding-energy component of the O 1s peak, attributed to increasing Al–O bonding. This indicated that Al could break both C–O bonds and abstract O atoms from the surface. The O content was also often higher than expected for 1 ML coverage, suggesting that Al was partly oxidized in air. This would be detrimental for NEA because it would form a C–O–Al–O bonding arrangement with an additional dipole at the surface with negative charge outermost. As such, it appears that the propensity for Al to bond with O is, in fact, rather disadvantageous for thermionic applications.

In general, these results broadly agree with computational predictions,<sup>[33,35]</sup> albeit with some caveats. Computer simulations suggest that the Al + O-terminated (100) and (111) diamond surfaces should have EAs of  $-0.4$  and  $-1.2$  eV, respectively, and have adsorption energies of  $\approx 6$ – $8$  eV per atom. Experimentally we found that, except for loss of excess O upon first heating, the Al + O surface remained stable up to  $800^\circ\text{C}$ , whereas the EA values were generally between  $0.0$  and  $-1.0$  eV, depending upon the deposition method, coverage, and annealing temperature. Care should be taken with these comparisons, however, as the simulations were for undoped diamond, whereas the experimental substrates had a boron-doped layer. In addition to changing the electrical conductivity of the bulk, dopants also produce band bending at the surface, and this can have a significant effect upon the magnitude and sign of the EA. Larsson<sup>[54]</sup> used density functional theory methods to calculate the EAs for a range of terminating species (H, O, OH, NH<sub>2</sub>, F) on undoped, p-doped, and n-doped diamond (100) and (111) surfaces. She found the EA values depended significantly upon all these factors: adsorbate, adsorbate geometry (e.g., linear or bridging), diamond surface orientation, and importantly, bulk doping type. Thus, care must be exercised when comparing experimental values with theoretical EA values

to ensure that these factors are known in each case. In this case, no theoretical calculations have yet been reported for Al + O-terminated BDD, and so these would be a useful next step.

It is clear that there was a wide variation in EA values obtained from the samples, even across the same wafer surface. One of the key issues here is the unreliability of forming a uniform O-terminated surface, where the oxygens are all in either the ketone- or ether-bridging positions. The different oxygenation methods not only sometimes produce incompletely oxidized surfaces, but also there is no control of the ratio of ketone-to-ether structures across the surface. This leads to patchy surfaces with areas of good electron emission performance with high NEA, adjacent to areas of poor performance with low NEA or even PEA. Optimization of the oxidation process to develop a method that preferentially produces only one type of oxygenated diamond surface would be a key goal to improve results. Reactions routine to organic chemistry to modify the type of bonding at the O-terminated surface, such as Pinacol coupling, diol-oxidation, or ether-cleavage reactions,<sup>[33]</sup> might also be worth pursuing. The work of Yoshida et al.,<sup>[55]</sup> where (111) diamond was heated in H<sub>2</sub>O vapor to selectively obtain hydroxyl-terminated diamond, appears to be the closest approach to date for the formation of a singular type of oxygen bonding on (111) diamond, so perhaps a similar procedure could be used to hydroxyl terminate the (100) surface.

Although the ALD and e-beam methods showed promising low work function and electron affinity values, these are expensive, time-consuming, and temperamental experiments to conduct and as such, would likely not be methods of choice for scaling up to real-life applications. The thick-film method, however, is readily scalable, but often suffers from poor reproducibility. Optimizing this process for different Al evaporation thicknesses, acid-washing conditions and different annealing strategies would be another useful strategy.

This study focused on Al deposition onto O-terminated diamond, but other studies should be undertaken to study Al termination on bare diamond. This might remove the issue of Al scavenging O, because O would no longer be present in this system; however, the drawback is that it might make the samples air sensitive.

Computational calculations of  $\leq 1$  ML Al on bare diamond<sup>[33,35,36]</sup> predict that the Al–diamond surface should be temperature stable, and that its NEA should become more negative with increasing Al coverage. It would be useful to confirm this and to understand how much Al can be deposited before the bulk properties of the metal dominate. Similarly, the time dependence of the EA and work functions of these films are yet to be studied. To produce usable thermionic devices, the surfaces must retain their NEA properties for periods of years under continual usage, and in common with many other diamond terminations, these long-term stability measurements are yet to be determined for AlO–diamond.

Other metal–oxygen terminations of diamond using Group I and II metals or selected TMs<sup>[1]</sup> have also shown, or been predicted to have, large NEAs and could be further optimized in future. Many other potential candidates have yet to be explored. Some of these metals are arguably more promising for thermionic applications as they benefit from being much more electro-positive than Al, while also demonstrating stability at thermionic temperatures. They also have weak metal–metal bonds, thus favoring ionic bonding to the diamond surface, rather than cross-linking to adjacent metal atoms on the surface. This would reduce recombination pathways for electrons, a potential factor that may hinder electron emission.

## Supporting Information

Supporting Information is available from the Wiley Online Library or from the author.

## Acknowledgements

M.C.J. thanks the Engineering and Physical Sciences Research Council (EPSRC) for funding under grant code EP/L016648/1 as part of the Functional Nanomaterials CDT. The authors acknowledge the Bristol NanoESCA Facility (funded by EPSRC Strategic Equipment Grants EP/K035746/1 and EP/M000605/1). The ALD work was developed within the scope of the project CICECO-Aveiro Institute of Materials, UIDB/50011/2020 and UIDP/50011/2020, financed by national funds through the Portuguese Foundation for Science and Technology/MCTES.

## Conflict of Interest

The authors declare no conflict of interest.

## Data Availability Statement

Raw data from these experiments can be found on the University of Bristol data repository: <https://doi.org/10.5523/bris.3ohhlefv13zr23pcl9u55a21f>.

## Keywords

aluminium termination, CVD diamond, negative electron affinity, thermionic emission, work function

Received: January 22, 2021

Revised: March 11, 2021

Published online:

- [1] M. C. James, F. Fogarty, R. Zulkharnay, N. A. Fox, P. W. May, *Carbon* **2020**, *171*, 532.
- [2] E. Monroy, F. Omnès, F. Calle, *Semicond. Sci. Technol.* **2003**, *18*, R33.
- [3] P. Ascarelli, E. Cappelli, F. Pinzari, C. Rossi, S. Salvatori, G. Merli, A. Migliori, *J. Appl. Phys.* **2001**, *89*, 689.
- [4] A. Shih, J. Yater, P. Pehrsson, J. Butler, C. Hor, R. Abrams, *J. Appl. Phys.* **1997**, *82*, 1860.
- [5] F. A. M. Koeck, R. J. Nemanich, A. Lazea, K. Haenen, *Diamond Relat. Mater.* **2009**, *18*, 789.
- [6] R. J. Hamers, J. A. Bandy, D. Zhu, L. Zhang, *Faraday Discuss.* **2014**, *172*, 397.
- [7] K. P. Loh, I. Sakaguchi, M. Nishitani-Gamo, T. Taniguchi, T. Ando, *Diamond Relat. Mater.* **1999**, *8*, 781.
- [8] R. J. Nemanich, P. K. Baumann, M. C. Benjamin, S. W. King, J. van der Weide, R. F. Davis, *Diamond Relat. Mater.* **1996**, *5*, 790.
- [9] J. B. Cui, J. Ristein, L. Ley, *Phys. Rev. Lett.* **1998**, *81*, 429.
- [10] J. Van Der Weide, Z. Zhang, P. K. Baumann, M. G. Wensell, J. Bernholc, R. J. Nemanich, *Phys. Rev. B* **1994**, *50*, 5803.
- [11] F. J. Himpsel, J. A. Knapp, J. A. VanVechten, D. E. Eastman, *Phys. Rev. B* **1979**, *20*, 624.
- [12] P. K. Baumann, R. J. Nemanich, *Surf. Sci.* **1998**, *409*, 320.
- [13] L. Diederich, O. M. Küttel, P. Aebi, L. Schlapbach, *Surf. Sci.* **1998**, *418*, 219.
- [14] W. F. Paxton, M. Howell, W. P. Kang, J. L. Davidson, *J. Vac. Sci. Technol. B* **2012**, *30*, 021202.
- [15] J. Raymakers, K. Haenen, W. Maes, *J. Mater. Chem. C* **2019**, *7*, 10134.
- [16] K. P. Loh, J. S. Foord, R. G. Egdell, R. B. Jackman, *Diamond Relat. Mater.* **1997**, *5*, 874.
- [17] K. P. Loh, X. N. Xie, S. W. Yang, J. S. Pan, P. Wu, *Diamond Relat. Mater.* **2002**, *11*, 1379.
- [18] K. W. Wong, Y. M. Wang, S. T. Lee, R. W. M. Kwok, *Appl. Surf. Sci.* **1999**, *140*, 144.
- [19] J. L. Nie, H. Y. Xiao, X. T. Zu, *Chem. Phys.* **2006**, *326*, 308.
- [20] P. K. Baumann, R. J. Nemanich, *Appl. Surf. Sci.* **1996**, *104–105*, 267.
- [21] P. K. Baumann, R. J. Nemanich, *J. Appl. Phys.* **1998**, *83*, 2072.
- [22] J. van der Weide, R. J. Nemanich, *J. Vac. Sci. Technol. B* **1992**, *10*, 1940.
- [23] A. K. Tiwari, J. P. Goss, P. R. Briddon, N. G. Wright, A. B. Horsfall, M. J. Rayson, *Phys. Status Solidi A* **2012**, *209*, 1697.
- [24] K. Tiwari, J. P. Goss, P. R. Briddon, A. B. Horsfall, N. G. Wright, R. Jones, M. J. Rayson, *Europhys. Lett.* **2014**, *108*, 46005.
- [25] K. M. O'Donnell, T. L. Martin, N. A. Fox, D. Cherns, *Phys. Rev. B* **2010**, *82*, 115303.
- [26] K. M. O'Donnell, T. L. Martin, N. L. Allan, *Chem. Mater.* **2015**, *27*, 1306.
- [27] K. M. O'Donnell, T. L. Martin, M. T. Edmonds, A. Tadich, L. Thomsen, J. Ristein, C. I. Pakes, N. A. Fox, L. Ley, *Phys. Status Solidi A* **2014**, *211*, 2209.
- [28] K. M. O'Donnell, M. T. Edmonds, A. Tadich, L. Thomsen, A. Stacey, A. Schenk, C. I. Pakes, L. Ley, *Phys. Rev. B* **2015**, *92*, 35303.
- [29] D. A. Evans, O. R. Roberts, A. R. Vearey-Roberts, D. P. Langstaff, D. J. Twitchen, M. Schwitters, *Appl. Phys. Lett.* **2007**, *91*, 132114.
- [30] T. Matsumoto, H. Kato, K. Oyama, T. Makino, M. Ogura, D. Takeuchi, T. Inokuma, N. Tokuda, S. Yamasaki, *Sci. Rep.* **2016**, *6*, 31585.
- [31] A. Maréchal, M. Aoukar, C. Vallée, C. Rivière, D. Eon, J. Pernot, E. Gheeraert, *Appl. Phys. Lett.* **2015**, *107*, 1.
- [32] A. Hiraiwa, T. Saito, D. Matsumura, H. Kawarada, *J. Appl. Phys.* **2015**, *117*, 215304.
- [33] M. C. James, PhD Thesis, University of Bristol, **2019**.
- [34] M. C. James, A. Croot, P. W. May, N. L. Allan, *J. Phys.: Condens. Matter* **2018**, *30*, 235002.
- [35] M. C. James, P. W. May, N. L. Allan, *J. Phys.: Condens. Matter* **2019**, *31*, 295002.
- [36] J. M. A. Beattie, J. P. Goss, M. J. Rayson, P. R. Briddon, *Diamond Relat. Mater.* **2019**, *94*, 137.

- [37] O. J. L. Fox, J. O. P. Holloway, G. M. Fuge, P. W. May, M. N. R. Ashfold, in *Diamond Electronics and Bioelectronics - Fundamentals to Applications III* (Eds: P. Bergonzo, J. E. Butler, R. B. Jackman, K. P. Loh, M. Nesládek), Mater. Res. Soc. Symp. Proc., Vol. 1203, MRS, Warrendale, PA **2010**, paper J17-27.
- [38] X. Zhang, PhD Thesis, University of Bristol, Bristol, UK, **2017**.
- [39] G. Wan, M. Cattelan, N. A. Fox, *J. Phys. Chem. C* **2019**, 123, 4168.
- [40] A. Jaggernauth, R. M. Silva, M. A. Neto, F. J. Oliveira, I. K. Bdikin, M. P. Alegre, M. Gutiérrez, D. Araújo, J. C. Mendes, R. F. Silva, *Surf. Coat. Technol.* **2020**, 397, 125991.
- [41] M. Z. Othman, PhD Thesis, University of Bristol, UK, **2014**.
- [42] T. Sun, PhD Thesis, Arizona State University, USA, **2013**.
- [43] A. Schenk, A. Tadich, M. Sear, K. M. O'Donnell, L. Ley, A. Stacey, C. Pakes, *Appl. Phys. Lett.* **2015**, 106, 191603.
- [44] M. J. Sear, A. K. Schenk, A. Tadich, B. J. Spencer, C. A. Wright, A. Stacey, C. I. Pakes, *J. Phys.: Condens. Matter* **2017**, 29, 145002.
- [45] J. J. Yeh, I. Lindau, *Atomic Calculation of Photoionization Cross-Sections and Asymmetry Parameters*, Gordon and Breach, Langhorne, PA **1993**.
- [46] G. Wan, S. Panditharatne, N. A. Fox, M. Cattelan, *Nano Express* **2020**, 1, 020011.
- [47] J. F. Moulder, W. F. Stickle, P. E. Sobol, K. D. Bomben, *Handbook of X-ray Photoelectron Spectroscopy*, Perkin-Elmer, Eden Prairie, MN **1992**.
- [48] S. Ghodbane, D. Ballutaud, A. Deneuve, C. Baron, *Phys. Status Solidi A* **2006**, 203, 3147.
- [49] A. K. Schenk, K. J. Rietwyk, A. Tadich, A. Stacey, L. Ley, C. I. Pakes, *J. Phys.: Condens. Matter* **2016**, 28, 305001.
- [50] K. Huang, X. Hu, H. Xu, Y. Shen, A. Khomich, *Appl. Surf. Sci.* **2014**, 317, 11.
- [51] G. Wan, M. Cattelan, N. A. Fox, *J. Phys. Chem. C* **2019**, 123, 4168.
- [52] F. Maier, J. Ristein, L. Ley, *Phys. Rev. B* **2001**, 64, 165411.
- [53] K. P. Loh, X. N. Xie, S. W. Yang, J. C. Zheng, *J. Phys. Chem. B* **2002**, 106, 5230.
- [54] K. Larsson, *J. Carbon Res.* **2020**, 6, 22.
- [55] R. Yoshida, D. Miyata, T. Makino, S. Yamasaki, T. Matsumoto, T. Inokuma, N. Tokuda, *Appl. Surf. Sci.* **2018**, 458, 222.